

A synthesis, characterization and catalytic application of CNT aerogels for conversion of β -nitrostyrenes to aryhydrazones

Hossein Tavakol* , Reza Goodarzi

Department of Chemistry, Isfahan University of Technology, Isfahan 84156-83111, Iran.

*Corresponding author: h.tavakol@iut.ac.ir

Original Research

Abstract:

Received:
28 April 2025
Revised:
16 June 2025
Accepted:
10 July 2025
Published online:
15 July 2025
Published in issue:
30 September 2025

In this study, carbon aerogel was first prepared via the reaction between carbon nanotubes and chitosan. The structure and properties of the prepared carbon aerogel were determined using FESEM, EDS, XRD, FTIR, Raman, TEM, and nitrogen adsorption-desorption isotherm (Based on BET theory). Through the various analyses of the aerogel, due to its mesoporous structure and enriched functional surface, the prepared aerogel was a suitable candidate for catalyzing the reaction. Moreover, there were a few reports on the direct use of carbon-based aerogels as a catalyst. Therefore, the reaction between β -nitrostyrene and hydrazine hydrate was considered for this purpose. This reaction is a retro-aza-Henry type reaction, including non-oxidative C=C double bond cleavage, which is a rare phenomenon in organic reactions. The optimized conditions were obtained using several experiments. Based on these experiments, the best result was obtained using 10 mL ethanol as solvent, 25 °C temperature, 30 mg catalyst, and two mmol hydrazine hydrate solution (80%), and in 3 h. According to our experiments, 11 different derivatives of β -nitrostyrene were successfully converted to the corresponding hydrazone in 95 – 99% yield. The catalyst showed promising results in the reusability experiments, where after six consecutive runs, the yield was reduced by only 5%.

© 2025 The Author(s). Published by the OICC Press under the terms of the [Creative Commons Attribution License](#), which permits use, distribution and reproduction in any medium, provided the original work is properly cited.

Keywords: Aerogel; Chitosan; CNT; Catalyst; β -nitrostyrene; Hydrazones

1. Introduction

Aerogels are mesoporous solids or ultra-porous polymer networks with very low densities ($0.004 - 0.500 \text{ gr}\cdot\text{cm}^3$) [1]. In simpler terms, an aerogel is a porous solid suspension in a solvent where the solvent has been replaced by a gas, resembling a sponge but thousands of times more porous. This high porosity is the reason for the extremely low density and high specific surface area of aerogels [2, 3]. The first aerogel was created in the late 1920s by Samuel Kistler, consisting of 90% empty space and having a specific surface area greater than $1000 \text{ m}^2/\text{gr}$. This aerogel was made from silica gel using the supercritical drying method, which will be discussed in more detail in subsequent sections [4]. Aerogels are categorized based on various factors [5]. The final form, synthesis method, and pore size are among the criteria used to classify aerogels [6]. For example, based on pore size, they can be divided into three groups: mesoporous (with pore sizes ranging from 2 to 50 nanometers),

microporous (with pore sizes less than 2 nanometers), and a third group that is a combination of mesoporous and microporous structures [7]. The most widely accepted classification of aerogels is based on the chemical composition used in them [8]. Accordingly, aerogels are generally classified into two main categories: single-component and multi-component or composite aerogels. Single-component aerogels are the most common type and include oxide aerogels (silica-based and non-silica-based), natural aerogels (cellulose-based), organic aerogels (such as graphene, carbon nanotubes, and other carbon-based compounds), chalcogenide aerogels (containing anions from group 16 elements of the periodic table), and other types of aerogels. The applications of aerogels cover a wide areas since due to their wide range of precursors, porous structure and shape, and synthesis methods, they have been employed in many applications such as electronics [9], photodegradation [10], gas absorption [11, 12], separation [13, 14], water purifica-

tion [15, 16], thermal insulation [17], oil/water separation [18], flame retardants [19, 20], catalysts [21], and catalyst support [22–24]. In this line, carbon-based aerogels showed high potencies in various fields, which makes them a promising material because they are the least expensive and least hazardous aerogels [25]. Among various applications of carbon aerogels, their catalytic activities have been of interest, especially by organic chemists [26]. The highly porous structure and various functional surfaces of these materials make them a suitable candidate for catalyzing chemical processes, as well as their utilization as a support for catalysts [27–30]. Moreover, they have very low densities, which allows the scientist to use a small amount of them and reduce the process costs [31]. However, despite these promising properties, there are a few studies related to the direct use of carbon aerogels as a catalyst, and they were employed mostly as a support for the catalysts, mostly in fuel cells [32–34]. As a first example for the direct use of carbon aerogels as a catalyst, Seredych et al. used them as a metal-free oxygen reduction catalyst [35]. In another study, electrochemical nitrate was used to reduce ammonia by using carbon aerogels as a catalyst [36]. Next, Tian and co-workers reported a KOH-activated N-doped novel carbon aerogel as an efficient metal-free oxygen reduction catalyst for microbial fuel cells [37]. Moreover, N-doped carbon aerogels were employed as a catalyst for the oxygen reduction reaction [38]. All the mentioned studies are related to the catalytic use of carbon aerogels in electrochemical processes, and there are very few examples of their catalytic use in simple chemical processes. In one of the rare studies, carbon black-derived graphene quantum dots were composited with carbon aerogel and employed as a reduction catalyst for the iodide/tri-iodide couple [39]. Therefore, it was decided to prepare carbon aerogels and use them as a catalyst in a chemical reaction. For this purpose, based on the previous studies of this group related to the preparation and utilization of carbon-based materials [40–42], the reaction between β -nitrostyrenes and hydrazine has been considered, because of our previous experience on the reactions of β -nitrostyrenes [43–45]. This reaction is known as the retro-aza-Henry reaction in the chemical literature. The first step of this reaction is a Michael addition reaction. The carbon aerogel can catalyze this reaction by accelerating the first Michael addition and facilitating the next steps, consisting of the proton-transfer and breaking the C-C bond, as will be displayed and discussed in the following sections. The most important advantages of this work are using metal-free and inexpensive catalysts in nearly green conditions to catalyze an interesting reaction. Moreover, there is no similar report related to this work, and this study opens a new horizon in this area.

2. Experimental

2.1 Materials and equipment

Carboxylated MWCNTs were bought from US Research Nanomaterials, Inc., USA. The Other starting materials, nitromethane, nitroethane, benzaldehyde derivatives, hydrazine hydrate ($N_2H_4 \cdot H_2O$), phosphoric acid (H_3PO_4), potassium permanganate ($KMnO_4$), and ammonium acetate,

were purchased from Merck, DaeJu, and Sigma Aldrich Co in synthetic grade. All of them were used without further purification. Solvents were bought from domestic companies in industrial grades and used after distillation. Freeze-drying experiments were performed using the JFD570 instrument, made by Zhal Teb, Tehran, Iran. The FESEM images were recorded using the Sigma 300 model of Zeiss, Germany. Raman spectra were acquired using a TakRam N1-541 spectrometer (Iran) at excitation of 532 nm. X-ray diffraction (XRD) measurement was determined by using a Philips PW-1730 diffractometer equipped with Cu-K α radiation ($\lambda = 0.1541$ nm). The thermogravimetric analysis (TGA) was performed under argon environments using TA Instruments Q600 from 25 °C to 600 °C at a heating rate of 10 °C/min. The adsorption-desorption diagrams and related surface properties were recorded using Belsorb mini II, made by Micotrac Bel Corp, Japan. FT-IR spectra were obtained from AVATAR, Thermo Fisher, USA. GC-Mass analyses were performed using an Agilent-5975C instrument.

2.2 Preparation of β -nitrostyrene and its derivatives

2.2.1 Preparation of β -nitrostyrene with electron donor groups

4 mL of methanol was added to a 100 mL Erlenmeyer flask, which was then put in an ice bath (The first step). Meanwhile, in a 5 mL beaker, 0.85 g of NaOH was dissolved in 1 mL of water, and the beaker was placed in an ice bath (The second step). Then, 19 mmol of benzaldehyde and 18 mmol of nitromethane were added to the primary Erlenmeyer (in the first step) under constant stirring. Following the solution prepared in step 2 was added slowly and dropwise to the Erlenmeyer at 5 °C and then placed on a stirrer for 20 min. Then, 10 mL of 4 M HCl was added to the reaction mixture. The prepared β -nitrostyrene was separated by filter paper, and recrystallization was used to purify the product (in EtOH solvent) [18].

2.2.2 Preparation of β -nitrostyrene with electron acceptor groups

First, in a 50 mL single-neck balloon, 20 mL of AcOH, 10 mL of nitromethane, 12 mmol of NH_4OAc , and 50 mmol of aldehyde were added, respectively. The resulting solution was stirred in an oil bath at 90 °C for 5 minutes under a magnetic stirrer. Finally, 20 mL of DW was added to the reaction mixture, and the separation of organic and aqueous components was performed with 50 mL of ethyl acetate in two stages. The resulting product was dried over Na_2SO_4 , and recrystallization was used to purify the product (in EtOH solvent) [19].

2.3 Preparation of carbon aerogels

2.3.1 Deacetylation of chitosan

The purchased chitosan was 80% deacetylated. To enhance the efficiency of chitosan as a crosslinking agent, it was further deacetylated through a reaction to increase this percentage. In this method, the secondary amide groups present in chitosan are converted into primary amine groups through a chemical reaction. To carry out this reaction, a 47% sodium

hydroxide solution was first prepared. Then, 30 g of chitosan was added to it, and the temperature of the suspension was raised to 110 °C using a heater. The chitosan suspension in the sodium hydroxide solution was stirred at this temperature for two hours. After the reaction was completed, the suspension was filtered, and the chitosan was separated. To reduce the pH of the chitosan, it was washed several times with distilled water to completely remove the residual base. The details of this reaction are shown in figure 1.

2.3.2 Synthesis of carbon aerogels from carboxylated MWCNTs

To synthesize carbon nanotube aerogel, 0.071 g of carboxylic acid-functionalized MWCNTs were first weighed and poured into a test tube containing 30 mL of deionized water. As previously mentioned, carbon-based compounds are difficult to disperse in water. Therefore, the test tube was placed in an ultrasonic bath for 30 min to enhance dispersion. After this step, the resulting suspension was placed on a magnetic stirrer at room temperature. While stirring, first 0.05 g of iron (III) chloride was added, and after one minute, 0.5 g of chitosan was added to the suspension. Stirring continued for one hour. After one hour, the viscosity of the suspension increased, which indicates crosslinking between the chitosan molecules and the nanotubes and the formation of a network structure, resulting in gelation. In

the next step, the prepared gel was poured into a glass Petri dish with a diameter of 10 cm and a depth of 1.5 cm. The formed gel was placed in a freezer at -4 °C for 48 h to completely freeze. Then, the frozen gel was placed in a freeze-dryer for 48 h so that the solvent (water) would be extracted from the aerogel network, yielding the final product (carbon nanotube aerogel). The resulting product was used directly as a catalyst in subsequent reactions without the need for purification.

2.4 General Procedure for the reaction of β -nitrostyrene with hydrazine using aerogel catalyst

Carbon aerogel (0.03 g), $N_2H_4 \cdot H_2O$ (3 mmol), β -nitrostyrene (1 mmol), and 10 mL of ethanol as a solvent were added to a 50 mL round-bottom flask. The flask was placed on a magnetic stirrer at room temperature to be stirred for three h. TLC analysis was used to track the course of the reaction (EtOAc: n-hexane, 1:1). After the reaction was completed (all reactant was consumed and only one spot was observed on the TLC plate), the catalyst and product were separated from the reaction mixture by filtration. The filtrate was washed with water (3 times) and cold ethanol (2 times), and then the organic part was solved in the minimum of hot ethanol to be recrystallized and purified for the next analyses. The yields were obtained by weighing the washed and dried filtrate (before recrystallization) and

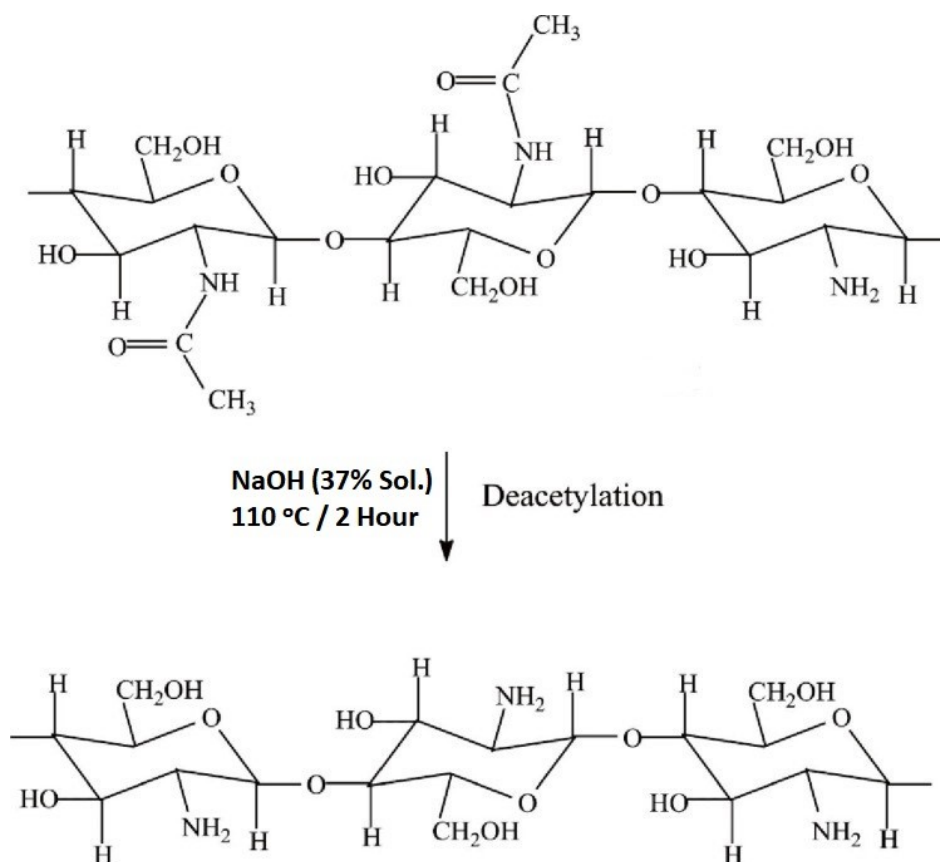


Figure 1. The reaction of the deacetylation of chitosan.

subtracting the weight of the catalyst.

2.5 The physical and spectroscopic data of the products

All products are known and their structures were confirmed by comparing their physical and spectroscopic data with the authentic references. The physical and spectroscopic data of the selected products are shown in this section. Moreover, original spectra were provided in the supporting information.

Benzylidenehydrazine (2a)

Yellow solid, melting point = 93-95 °C; IR (KBr): $\nu(\text{cm}^{-1})$: 3401 (N-H), 2914 (C-H), 1605 (C=N); $^1\text{H NMR}$ (400 MHz, CDCl_3) δ (ppm) = 8.72 (s, 1H, H-2), 7.87-7.93 (m, 2H, H-4), 7.49 (dd, $J = 5.0, 1.9$ Hz, 3H, H-5/6); $^{13}\text{C NMR}$ (100 MHz, CDCl_3) δ (ppm) = 162.1 (C-2), 134.1 (C-3), 131.2 (C-6), 128.8 (C-4), 128.6 (C-5). Mass analysis (EI); $m/z = 120.0, 93.0, 77.0, 51.0, 28.0$.

4-BromoBenzylidenehydrazine (2b)

With a solid, 95% yield (189 mg). Melting point = 66-70 °C; IR (KBr): $\nu(\text{cm}^{-1})$: 3401 (N-H), 2925 (C-H), 1603 (C=C), 505 (C-Br); $^1\text{H NMR}$ (400 MHz, CDCl_3) δ (ppm) = 8.62 (s, 1H, H-2), 7.74 (d, $J = 8.5$ Hz, 2H, H-4), 7.62 (d, $J = 8.5$ Hz, 2H, H-5), 5.99 (s, 2H, H-1); $^{13}\text{C NMR}$ (100 MHz, CDCl_3) δ (ppm) = 161.3 (C-2), 132.8 (C-3), 132.2 (C-5), 130(C-4), 125.9 (C-6).

N,N-Dimethylbenzylidenehydrazine (2c)

Yellow solid, melting point = 69-72 °C; IR (KBr): $\nu(\text{cm}^{-1})$: 3398 (N-H), 2919 (C-H), 1601 (C=C); $^1\text{H NMR}$ (400 MHz, CDCl_3) δ (ppm) = 8.6 (s, 1H, H-2), 7.77-7.71 (m, 2H, H-4), 6.87-6.73 (m, 2H, H-5), 3.06 (s, 6H, H-7); $^{13}\text{C NMR}$ (100 MHz, CDCl_3) δ (ppm) = 160.8 (C-6), 152.2 (C-2), 129.93 (C-4), 122.2 (C-3), 111.7 (C-5), 40 (C-7); Mass analysis (EI); $m/z = 163.2, 145.1, 121.1, 105.1, 77.1, 62.1, 42.1$.

4-Methoxybenzylidenehydrazine (2d)

Yellow oil, IR (KBr): $\nu(\text{cm}^{-1})$: 3362 (N-H), 3288 (N-H), 1599 (C=N), 785, 694; $^1\text{H NMR}$ (400 MHz, CDCl_3): δ 8.59 (s, 1H), 7.83 (d, $J = 8.2$ Hz, 2H), 7.04 (d, $J = 8.2$ Hz, 2H), 3.82 (s, 3H); $^{13}\text{C NMR}$ (100 MHz, CDCl_3): δ 161.7, 160.5, 129.9, 126.4, 116.3, 55.3; Mass analysis (EI); $m/z = 150.0, 122.0, 105.0, 90.9, 77.0, 58.0, 44.0, 28.0, 18.0$.

2,6-Dichlorobenzylidenehydrazine (2e)

White crystal, melting point = 134 °C; IR (KBr): $\nu(\text{cm}^{-1})$: 3401 (N-H), 2915 (C-H), 1598 (C=C); $^1\text{H NMR}$ (400 MHz, CDCl_3) δ (ppm) = 7.94 (s, 1H, H-2), 7.34 (d, 2H, $J = 8.1$ Hz, 2H, H-5), 7.16 (dd, $J = 8.5, 7.6$ Hz, 1H, H-6), 5.58 (s, 2H, H-1); $^{13}\text{C NMR}$ (100 MHz, CDCl_3) δ (ppm) = 137.4 (C-2), 134.6 (C-4), 131.2 (C-3), 129.2 (C-6), 128.8 (C-5); Mass analysis (EI); $m/z = 188.0, 170.9, 153.0, 136.0, 117.0, 90.0, 75.0, 63.0, 43.0, 28.0$.

3-Nitrobenzylidenehydrazine (2f)

Yellow crystal, melting point = 107.5-109.5 °C; IR (KBr): $\nu(\text{cm}^{-1})$: 3998 (N-H), 2917 (C-H), 1598 (C=C); $^1\text{H NMR}$

(400 MHz, CDCl_3) δ (ppm) = 8.39 (t, 1H, $J = 2.0$ Hz, H-2), 8.15 (ddd, 1H, $J = 8.3, 2.3, 1.1$ Hz, H-4), 7.90 (dt, 1H, $J = 7.8, 1.4$ Hz, H-8), 7.79 (s, 1H, H-6), 7.53 (t, 1H, $J = 8.0$ Hz, H-7), 5.79 (s, 1H, H-2); $^{13}\text{C NMR}$ (100 MHz, CDCl_3) δ (ppm) = 140.6 (C-5), 139.3 (C-2), 137.1 (C-3), 131.4 (C-8), 129.5 (C-7), 122.9 (C-6), 120.8 (C-4).

4-Nitrobenzylidenehydrazine (2g)

Yellow crystal, melting point = 134-135 °C; IR (KBr): $\nu(\text{cm}^{-1})$: 3401 (N-H), 2911 (C-H), 1608 (C=C), 1498 (N-O); $^1\text{H NMR}$ (400 MHz, CDCl_3) δ (ppm) = 8.26-8.19 (m, 2H, H-5), 7.76 (s, 1H, H-2), 7.72-7.63 (m, 2H, H-4), 5.90 (s, 2H, H-1); $^{13}\text{C NMR}$ (100 MHz, CDCl_3) δ (ppm) = 147.4 (C-6), 141.6 (C-2), 139 (C-3), 126.4 (C-4), 124 (C-5).

Pyridin-2-ylmethylenehydrazine (2h)

Yellow crystal, melting point = 148-150 °C; IR (KBr): $\nu(\text{cm}^{-1})$: 3399 (N-H), 2899 (C-H), 1602 (C=C); $^1\text{H NMR}$ (400 MHz, CDCl_3) δ (ppm) = 8.74-8.71 (m, 1H, H-7), 8.68 (s, 1H, H-2), 8.12 (dt, $J = 8.0, 1.1$ Hz, 1H, H-4), 7.79 (td, $J = 7.7, 1.8$ Hz, 1H, H-5), 7.35 (ddd, $J = 7.6, 4.9, 1.2$ Hz, 1H, H-6); $^{13}\text{C NMR}$ (100 MHz, CDCl_3) δ (ppm) = 162.3 (C-3), 152.9 (C-7), 150 (C-2), 136.6 (C-5), 125.2 (C-6), 122.6 (C-4).

Furan-2-yl-methylenehydrazine (2i)

Dark brown solid, melting point = 98-100 °C; IR (KBr): $\nu(\text{cm}^{-1})$: 3402 (N-H), 3056 (C-H), 1629 (C=C), 1005 (C-O), 1021 (N-N); $^1\text{H NMR}$ (400 MHz, CDCl_3) δ (ppm) = 8.50 (s, 1H, H-2), 7.56 (d, 1H, $J = 1.8$ Hz, H-6), 6.86 (dd, 1H, $J = 3.5, 0.8$ Hz, H-4), 6.49 (dd, $J = 3.5, 1.8$ Hz, 1H, H-5); $^{13}\text{C NMR}$ (100 MHz, CDCl_3) δ (ppm) = 150.9 (C-2), 149.4 (C-3), 145.8 (C-6), 115.8 (C-4), 112.3 (C-5); Mass analysis (EI); $m/z = 110.0, 93.0, 81.1, 68.0, 53.1, 39.1, 28.1$.

Naphthalene-1-ylmethylenehydrazine (2j)

White crystal, melting point = 88-90 °C; IR (KBr): $\nu(\text{cm}^{-1})$: 3401 (N-H), 2910 (C-H), 1599 (C=C); $^1\text{H NMR}$ (400 MHz, CDCl_3) δ (ppm) = 7.93 (s, 1H, H-2), 7.91-7.80 (m, 5H, H-12/H-10/H-11/H-8/H-5), 7.58-7.41 (m, 2H, H-6/H-7), 5.62 (s, 2H, H-1); $^{13}\text{C NMR}$ (100 MHz, CDCl_3) δ (ppm) = 143.3 (C-2), 133.7 (C-9), 133.4 (C-4), 132.8 (C-3), 128.4 (C-10), 128.1 (C-8), 127.8 (C-11), 126.7 (C-12), 126.4 (C-6), 126.3 (C-7), 122.9 (C-5); Mass analysis (EI); $m/z = 170.2, 154.1, 127.1, 101.1, 77.1, 51.1, 28.1$.

4-Chlorobenzylidenehydrazine (2k)

Yellow solid, melting point = 187-192 °C; IR (KBr): $\nu(\text{cm}^{-1})$: 3402 (N-H), 2911 (C-H), 1601 (C=C), 811 (C-Cl); $^1\text{H NMR}$ (400 MHz, CDCl_3) δ (ppm) = 8.62 (s, 1H, H-2), 7.80 (d, 2H, $J = 8.4$ Hz, H-4), 7.45 (d, $J = 8.5$ Hz, 2H, H-5), 5.81 (s, 2H, H-1); $^{13}\text{C NMR}$ (100 MHz, CDCl_3) δ (ppm) = 161.5 (C-2), 138 (C-6), 131.8 (C-3), 130.2 (C-4), 129.3 (C-5); Mass analysis (EI); $m/z = 154.1, 138.0, 127.1, 111.0, 92.1, 75.1, 63.1, 50.1, 39.1, 28.1$.

3. Results and Discussion

3.1 Synthesis and characterization of the CNT-based carbon aerogels

In this research, after the synthesis of the carbon nanotube aerogel catalyst, the reduction reaction of beta-nitrostyrene and its derivatives was carried out. In this reaction, the parameters of temperature, time, amount of hydrazine hydrate, amount of catalyst, and atmosphere were varied for optimization, which will be discussed further. Finally, after finding the optimal conditions for the reduction reaction of beta-nitrostyrene, its other derivatives were reacted under the most optimal conditions. Subsequently, the identification and analysis of the catalyst and the reactions performed will be discussed.

In the previous section, the practical method of catalyst synthesis was described. In the synthesis reaction of this catalyst, iron(III) chloride was used. Iron(III) chloride acts as a catalyst in this reaction, which, after accepting a free pair of electrons on the oxygen of the carbonyl group, increases the electrophilicity of the attached carbon and prepares it for nucleophilic attack (in this case, the chitosan amine group), as described in the previous report [46]. This reaction has a relatively high rate, and the viscosity of the suspension increases rapidly.

After the synthesis of the carbon nanotube aerogel catalyst, it was observed to have elastic properties and a very low density, like a sponge, which physically indicates the occurrence of the cross-linking reaction and the formation of the aerogel. To ensure the correct synthesis of the catalyst, analyses such as FESEM, RAMAN, BET, IR, XRD, TGA,

EDS, and MAP were performed, which will be discussed further.

The FESEM images and EDS analysis of the prepared aerogel are shown in figure 2. The FESEM images, which were provided in two different resolutions (10 and 200 μm), show a honeycomb structure via a 3D network consisting of thin walls and large cavities. The structure is a three-dimensional porous network. The pores are interconnected, which is crucial for applications such as a catalyst. The pores appear to be relatively uniform in size, though with some variation. The scale bar (200 μm) suggests pores range in the tens to hundreds of microns. Moreover, high porosity is evident, which is beneficial for catalytic use. The higher magnification image (right image) shows ultra-thin walls or membranes between pores. These walls have smooth surfaces and varying thickness, with some showing signs of nanofibrous structure or sheet-like formations. We can also see smaller pores or defects within the thin films. This might affect mechanical properties or permeability. The EDS analysis shows 47.79% carbon, 26.14% nitrogen, and 25.80% oxygen (all in atomic percent) and very small amounts of Fe (because of using ferric chloride as a catalyst of the crosslinking process) and Ni (0.02%, as an impurity during the synthesis of CNTs). The presence of oxygen and nitrogen is due to the chitosan chains, and this analysis confirms the preparation of the desired aerogels. To show the uniform distribution of all atoms in the structure of aerogel, the elemental mapping analyses for carbon, nitrogen, oxygen, iron, and nickel elements were performed, as they are shown in figure 3. These images confirm our guess about the formation of aerogel with a nearly uniform distribution

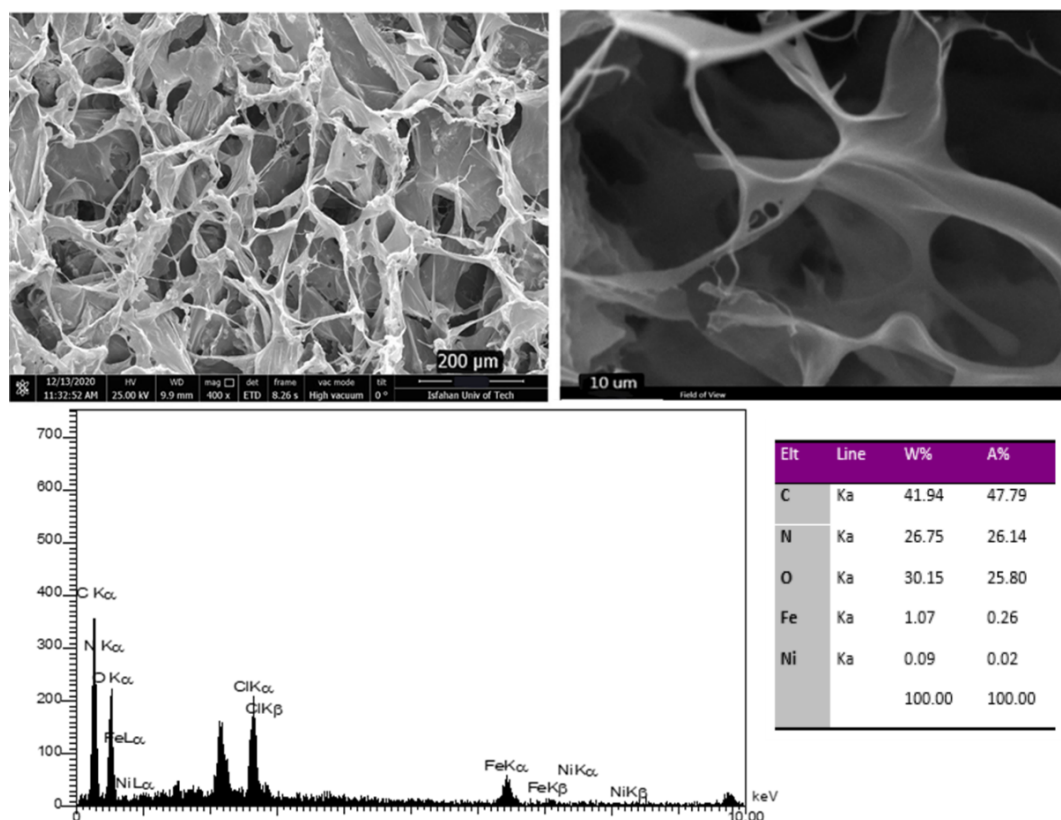


Figure 2. The FESEM images (in two different resolutions, top) and EDS analysis(below) of the prepared aerogel.

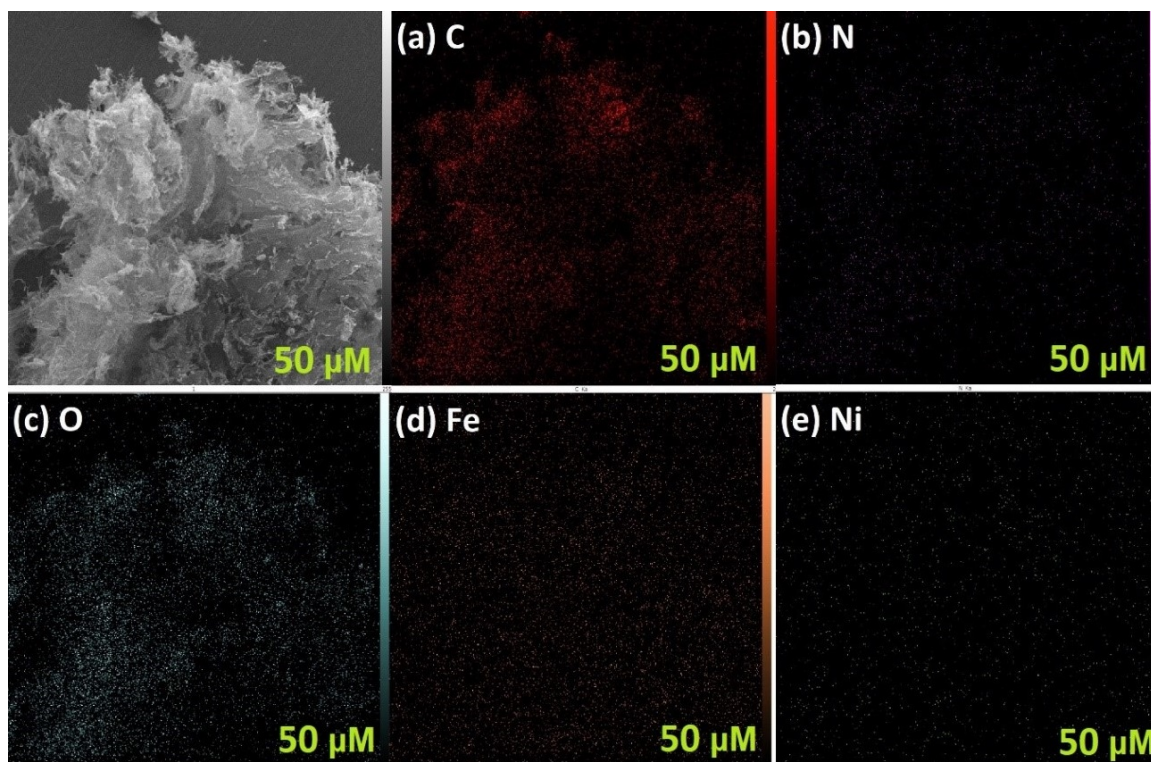


Figure 3. The elemental mapping analysis of the prepared aerogel.

of all mentioned elements. Moreover, the distribution of carbon and oxygen atoms is very similar to each other and like the authentic FESEM image (top left image).

The X-ray diffraction patterns of chitosan, pure carbon nanotubes, and prepared aerogel are shown in figure 4. In the chitosan diffraction pattern, a broad peak is observed in the range of 20 degrees, and this broadness indicates the amorphous nature of chitosan [47]. In the X-ray diffraction pattern of carbon nanotubes, a sharp peak with high

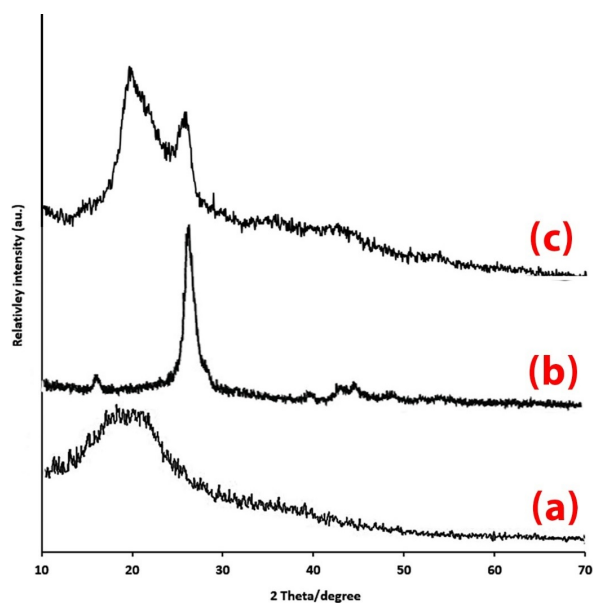


Figure 4. The XRD patterns of chitosan (a), carboxylated CNT (b), and chitosan-CNT aerogel (c).

intensity at an angle of 26 degrees, indicating the diffraction from the (002) graphitic planes, is observed. Additionally, a small peak is seen at an angle of 45 degrees, representing the diffraction from the (100) graphitic planes [48]. In the X-ray diffraction pattern after cross-linking between chitosan and carbon nanotubes, which is shown alongside the two mentioned patterns, a sharp peak is still observed at an angle of 25.5 degrees, indicating the presence of carbon nanotubes within the aerogel. This suggests a good crystalline form of the aerogel, and the change in the distance between the planes has caused a shift in the 2θ angle, which indicates cross-linking. Furthermore, the observation of this peak suggests that even after cross-linking, the structure of the nanotubes significantly influences the structure of the aerogel. The intensity of this peak has also changed after cross-linking with chitosan, which is evidence of bonding between these two molecules, accompanied by a phase change in the carbon nanotubes. Another sharp peak is observed at an angle of 20 degrees, indicating the presence of chitosan that has taken a crystalline form and is no longer amorphous. In the diffraction pattern obtained from the catalyst, there are no other additional peaks, indicating the purity of this catalyst.

FT-IR analysis was used to identify the functional groups of the catalyst. For this purpose, the FT-IR spectra of carbon nanotubes functionalized with carboxylic acid groups, chitosan, and the final aerogel were obtained, as they are shown in figure 5. In the spectrum of the carboxylated CNT (b) functionalized with carboxylic acid, a broad band is prominent in the range of $3500 - 3200 \text{ cm}^{-1}$, indicating the stretching vibrations of the acidic (-OH) group. It also shows a band at 1723 cm^{-1} , which is characteristic of the

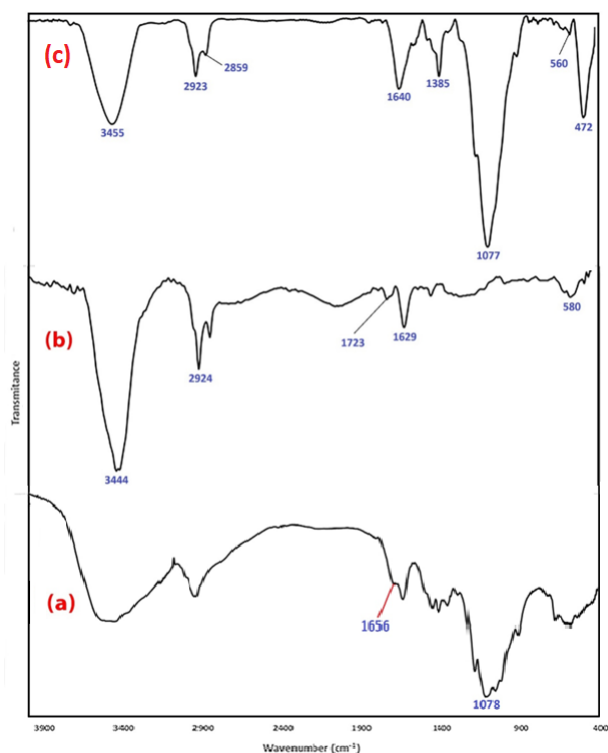


Figure 5. The FTIR spectra of chitosan (a), carboxylated CNT (b), and chitosan-CNT aerogel (c).

C=O stretching of the carboxylic acid group. In the spectrum of the synthesized aerogel, as mentioned earlier in the mechanism of the cross-linking reaction between nanotubes and chitosan, the most important functional group indicating cross-linking is the amide functional group. In the synthesized aerogel (c), a secondary amide (-NHR) is formed, which gives a band in the range of 1650 – 1580 cm^{-1} corresponding to the C=O stretching vibrations of the amide group. In this spectrum, a band is clearly visible at 1640 cm^{-1} . The broadband present at 3455 cm^{-1} corresponds to the stretching vibrations of -NH and -OH present in the catalyst, which overlap with each other. The band at 1385 cm^{-1} is related to the bending vibration of the -NH bond. Additionally, a high-intensity band is observed at 1077 cm^{-1} , which corresponds to the ether functional group (C-O stretching vibration), and the band at 1385 cm^{-1} indicates -OH bending, which is related to the cross-linked chitosan. The FT-IR spectrum of chitosan after deacetylation is shown in the figure above (a). The band related to the carbonyl functional group is visible with low intensity, indicating sufficient deacetylation.

One of the important analyses for investigating and measuring the total surface area of porous solids is the adsorption-desorption analysis. The basis of this analysis is the adsorption of inert gas molecules such as nitrogen and argon at various pressures on the surface of the pores of porous solids. The nitrogen adsorption-desorption analyses of the prepared aerogel, based on BET theory, were performed, and the results (including adsorption-desorption diagram, BJH curve, and t-plot analysis) were depicted in figure 6. The results are reported in the form of graphs showing the adsorption and desorption of gas molecules at different pressures, using

which information such as the type of pores, specific surface area, total pore volume, shape and type of existing pores, and pore size distribution can be obtained. According to the adsorption-desorption diagram (top) in this figure and by comparison with the IUPAC-defined standards, this aerogel falls into category V, which indicates that the catalyst is mesoporous. Also, in this analysis, the specific surface area was measured to be 23 m^2/g , and the average pore diameter was 20 nm. Furthermore, by using the hysteresis loop, the shape and type of pores present in the aerogel are determined. According to the adsorption-desorption isotherm, this catalyst is of type V, which indicates the presence of mesopores in the structure of the carbon nanotube aerogel. The BJH plot (below left) is used to determine the pore size, and according to its curve, the pore size distribution is in the range of 2 – 7 nm and 16 – 100 nm. Considering the range of pore diameters, it can be concluded that the aerogel has meso- and macropores. The last part of this analysis is the t-plot diagram, which is shown on the below right of figure 6 below. This plot is based on the Shull method, and by comparison with its standards, type III is confirmed, indicating the presence of mesopores in the aerogel structure. Figure 7 shows the TGA analysis plot of the carbon nanotube aerogel catalyst. This analysis is used to measure the thermal resistance of solid materials, and its working principle is the reduction in the mass of the solid material during an increase in temperature in an inert atmosphere. The heating rate used in this analysis was 10 $^{\circ}\text{C}/\text{min}$, and the analysis was performed under an argon atmosphere. After starting the analysis at room temperature up to 100 $^{\circ}\text{C}$, an 8% mass loss is observed in the aerogel. Due to the mesoporous structure of the synthesized aerogel, moisture can easily be absorbed into its pores. This 8% weight loss indicates the removal of interstitial moisture present in the mesopores of the aerogel. After increasing the temperature to 220 $^{\circ}\text{C}$, no change in the catalyst mass is observed, indicating the good thermal stability of this aerogel. From 220 to 320 $^{\circ}\text{C}$, a 30% mass loss is observed in the catalyst, which indicates the decomposition of the functional groups present on the carbon nanotubes and the chitosan molecules attached to them that remained free and unreacted. According to existing reports, chitosan experiences a 50% mass loss from 250 to 350 $^{\circ}\text{C}$, which, after cross-linking with carbon nanotube molecules, has decreased to 32%, indicating an increase in their stability after reaction with the nanotubes. Finally, from 320 to 720 $^{\circ}\text{C}$, the mass of the catalyst decreases rapidly, and this mass loss is related to the decomposition of the chitosan molecules attached to the nanotubes. From this analysis, it can be concluded that the carbon nanotube aerogel catalyst has relatively high resistance because it does not experience any significant mass loss other than the loss of interstitial moisture up to 220 $^{\circ}\text{C}$. As the last analysis of the prepared aerogel, Raman analysis is one of the useful analyses for investigating carbon structures, which identifies carbon structural defects as well as the amount of sp^2 hybridized carbon. In Raman analysis, all carbon compounds are characterized by two indicative bands, D and G, with different intensities and shifts. Figure 8 (top) shows the Raman analysis plot of carboxylated

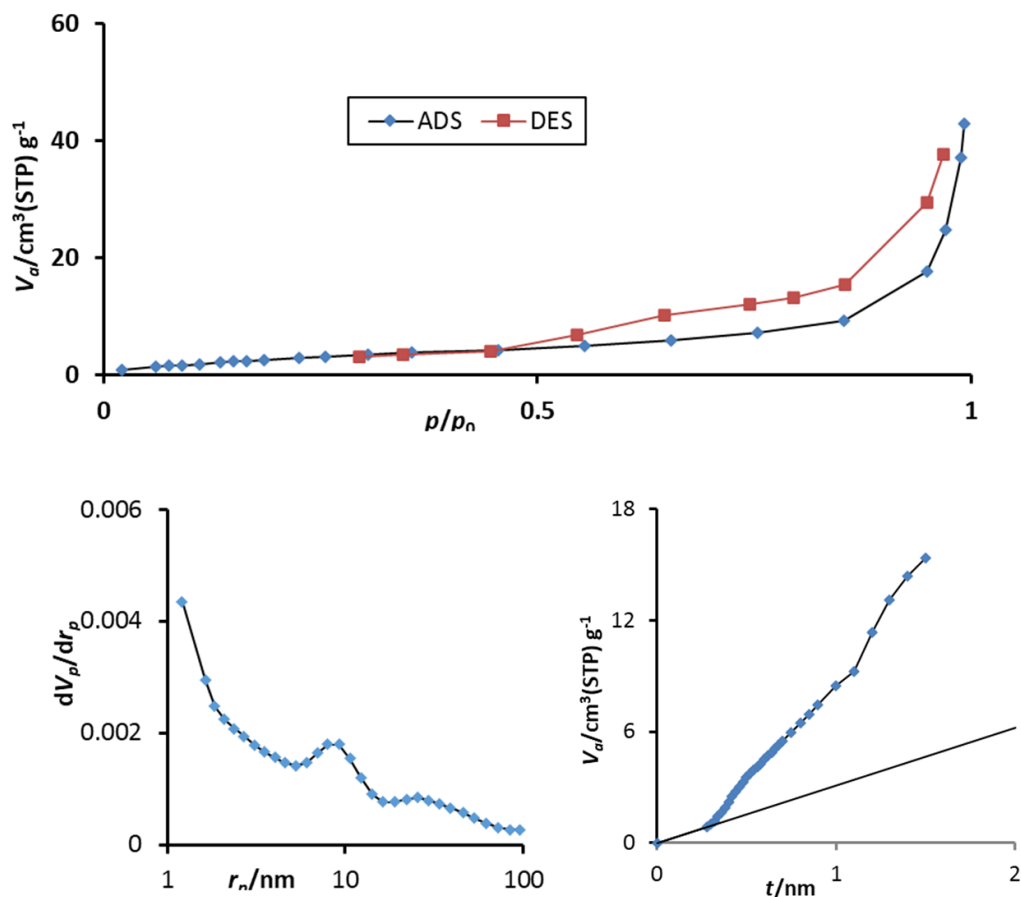


Figure 6. The adsorption-desorption diagram (top), BJH curve (below left) and t-plot analysis (below right) of the prepared aerogel.

carbon nanotubes, in which two indicative bands are observable. The band with a shift at 1350 cm^{-1} is the D band, and the band at 1583 cm^{-1} is the G band of this carbon allotrope. The existing D band indicates defects in the graphitic lattice structure and the vibrational modes of sp^3 hybridized carbon stretching. This disorder and defect are evidence of the presence of functional groups (the carboxylic acid functional group present in the nanotubes after oxidation). The G band present in the plot also indicates the hexag-

onal structure present in the nanotube network, which is due to the stretching vibration of the E_{2g} transitions of the graphitic lattice. The intensity ratio of the D to G band (I_D/I_G) in the carbon nanotubes was measured to be 0.8. The part below figure 8 shows the Raman analysis plot of the carbon nanotube aerogel catalyst. The intensity ratio of the D to G band for this catalyst was measured to be 0.9. The increase in this ratio indicates an increase in structural defects and chemical bonds, which can be attributed to the

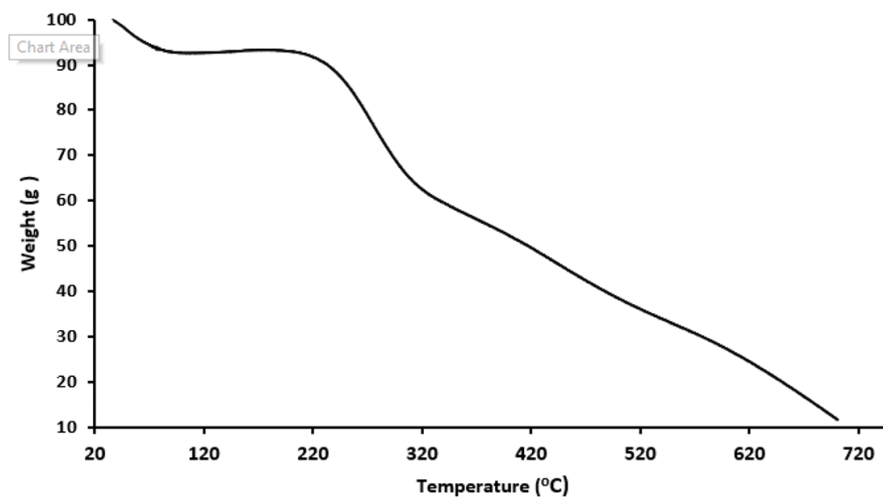


Figure 7. The TGA analysis of the prepared aerogel.

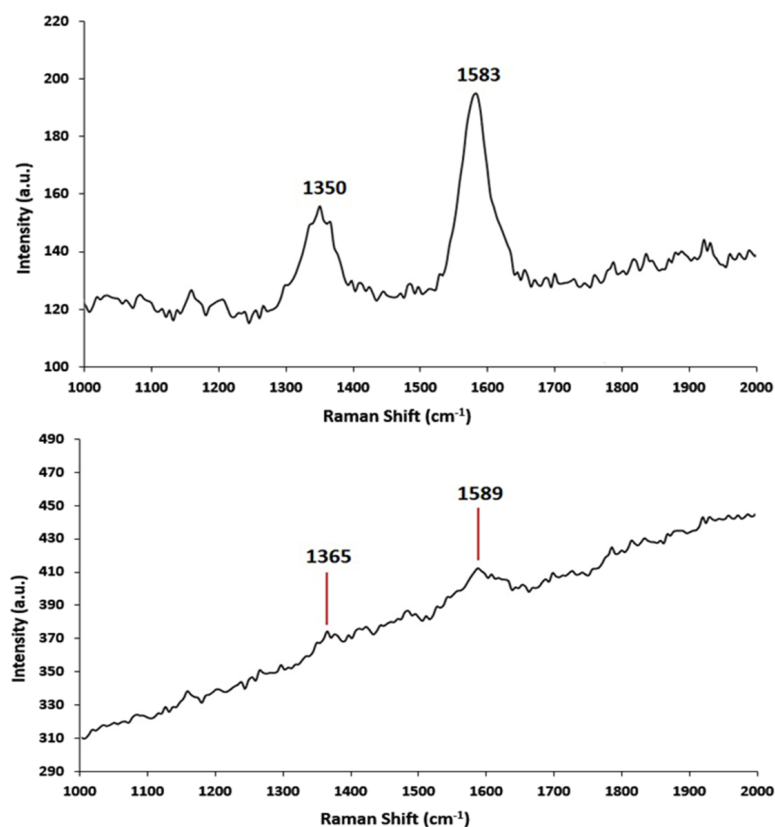


Figure 8. The Raman analyses of carboxylated CNT (top) and prepared aerogel (below).

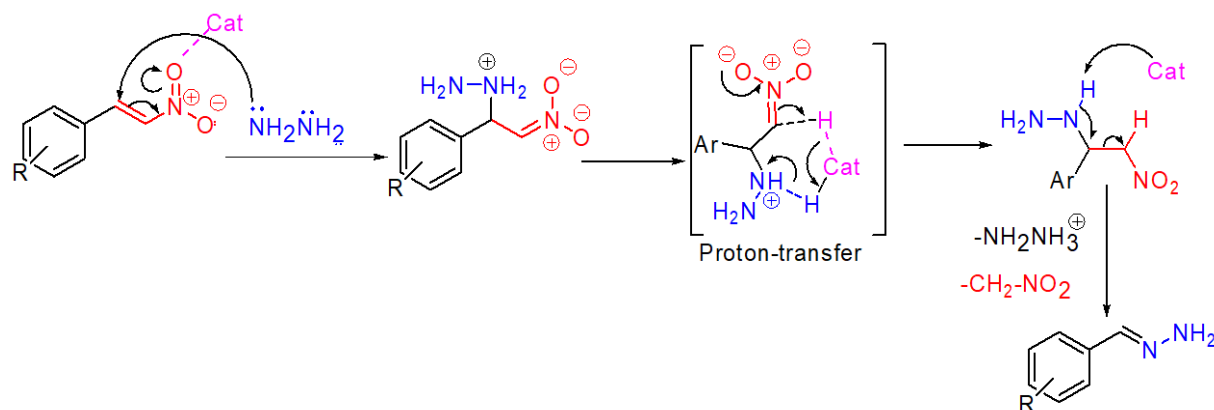
cross-linking between chitosan and nanotube molecules.

3.2 Catalytic performance of the prepared aerogel

After the successful synthesis and full characterization of the CNT-chitosan aerogel, it was employed as a catalyst in the reaction between β -nitrostyrenes and hydrazine hydrate. The reaction proceeded via a retro-aza-Henry type reaction to produce the corresponding hydrazone. The mechanistic details of this reaction are shown in scheme 1. This is an interesting reaction because of performing C=C double bond cleavage, which is a rare phenomenon in organic reactions. The employed catalysts (CNT-chitosan aerogel) have active Lewis's acid and Lewis's base sites that can activate the

nitrostyrene against the nucleophilic attack (the first step at scheme 1), facilitate the proton transfer in the second step, and help to detach the proton from the nitrogen in the hydrazine structure via the third step, as they described in scheme 1.

As the first step of the performing catalytic study, the reaction conditions were optimized using a model reaction, consisting of 1 mmol of β -nitrostyrenes, hydrazine hydrate (different amounts), aerogel catalyst (different amounts) in 10 mL of ethanol as a solvent. The results of the optimization processes were listed in Table 1. The amount of catalyst, the amount of hydrazine hydrate, the reaction temperature, and the reaction times are the parameters that



Scheme 1. The mechanistic details of the retro-aza-Henry type reaction between β -nitrostyrenes and hydrazine hydrate.

Table 1. The results of optimization of the model reduction^a.

Entry	Catalyst (mg)	Hydrazine (mmol)	Time (h)	Temp. (°C)	Yield (%) ^b
Optimization of the catalyst's amount					
1	–	2	3	Reflux	70
2	10	2	3	Reflux	80
3	30	2	3	Reflux	100
4	50	2	3	Reflux	100
5	70	2	3	Reflux	95
6	80	2	3	Reflux	90
Optimization of the hydrazine hydrate amount					
7	30	1	3	Reflux	90
8	30	2	3	Reflux	100
9	30	3	3	Reflux	85
Optimization of the reaction temperature					
10	30	2	3	50	100
11	30	2	3	25	100
Optimization of the reaction time					
12	30	2	1	25	75
13	30	2	3	25	100
14	30	2	6	25	100

^a The model reaction consists of 1 mmol of β -nitrostyrenes, hydrazine hydrate (different amounts), aerogel catalyst (different amounts) in 10 mL ethanol as a solvent. ^b The yields were obtained by weighting the product.

have been considered for optimization. To optimize the amount of catalyst, 0 – 80 mg of catalyst was employed in 6 different reactions (using 2 mmol of hydrazine, at reflux condition in 3 h, entries 1 – 6) and the best result was obtained using 30 mg of the catalysts (entry 3, defined with the bold font). To obtain the best amount for hydrazine hydrate, three experiments with 1, 2, and 3 mmol of hydrazine hydrate were designed (using 30 mg of catalyst, at reflux conditions in 3 h, entries 7 – 9), and the highest yield was observed during the use of 2 mmol hydrazine hydrate. For the optimization of the reaction temperature, in addition to the reflux condition, to more temperatures (25 and 50 °C) were employed in the next two experiments (using 30 mg of catalyst, 2 mmol hydrazine in 3 h, entries 10 and 11). Surprisingly, all reactions gave 100% yield. Therefore, the lowest temperature (25 °C) was selected as the optimized temperature. The last optimization was the reaction time, and 1, 3, and 6 hours were examined as the reaction time (using 30 mg of catalyst, 2 mmol hydrazine at 25 °C, entries 12 – 14). The 3 hours was selected as the optimized reaction time.

After the optimization of the reaction conditions and to show the generality and versatility of the presented reaction and the ability of the prepared aerogel catalyst, these optimized conditions were examined for the synthesis of other hydrazine derivatives, starting from different β -nitrostyrene derivatives. The results of these experiments in accordance with the general reaction were listed in Table 2. According

to this table, high yields are observed for all 11 derivatives (95 – 99%). The yields were obtained by weighting the washed and dried filtrate (before recrystallization) and subtracting the weight of the catalyst. The results show the high catalytic ability of the prepared aerogel in catalyzing this reaction. According to our experiments, 11 different derivatives of β -nitrostyrene were successfully converted to the corresponding hydrazone via the reaction with hydrazine hydrate using 3 mL of ethanol as a solvent, 30 mg of prepared aerogel as a catalyst, at room temperature in 3 h. Different electron-donor and electron acceptor groups on the phenyl ring (at different positions), as well as haloaromatic rings (pyridine and furan) and a polycyclic ring (naphthalene), were employed in this reaction. Since all yields are almost quantitative, the aryl substituent has a net meaningful effect on the reaction, and the reaction can be accomplished with any substituent. They may be rise from the high ability of the presented procedures and the potency of the catalyst, so that even the negative factors cannot have important effect on the reaction.

In the last part of this study, to examine the reusability of the catalyst, the separated, washed, and dried catalyst was first weighed, and no weight loss was observed, and then, it was reused for consecutive 5 more runs of the model reaction. Surprisingly, the yield was only reduced by 5%. This experiment showed the high recyclability and reusability of the prepared catalyst, as well as its high stability.

Finally, it is interesting to compare this study with the pre-

Table 2. The result of performing the reaction with different β -nitrostyrene derivatives.

$\text{Ar}-\text{CH}=\text{CH}-\text{NO}_2 \xrightarrow[10 \text{ mL ethanol, } 25^\circ\text{C, } 3\text{h}]{30 \text{ mg Cat, } 2 \text{ eq N}_2\text{H}_4} \text{Ar}-\text{CH}=\text{N}-\text{NH}_2$				
No	Ar	m.p. (Obs.)	m.p. (rep.)	Yield (%) ^a
2a	C ₆ H ₅ -	93-95	95	99
2b	4-Br-C ₆ H ₄ -	66-70	67-69	99
2c	4-NMe ₂ -C ₆ H ₄ -	69-72	70-71	99
2d	4-MeO-C ₆ H ₄ -	Oil	Oil	99
2e	2,6-dichloro-C ₆ H ₄ -	134	134	95
2f	3-NO ₂ -C ₆ H ₄ -	108-110	109	99
2g	4-NO ₂ -C ₆ H ₄ -	134-135	135	99
2h	2-pyridyl	148-150	150	95
2i	2-furyl	98-100	99-100	95
2j	1-naphthyl	88-90	89	99
2k	4-Cl-C ₆ H ₄ -	187-192	189-191	99

^a Isolated yields before recrystallization.

viously reported investigations. According to the literature review, only two similar works have been reported (one of which belonged to this group), and the results of the reported study were compared with our work in Table 3. From this table, the most savings in time and energy (related to the reaction temperature) and the highest possible yields can be found. The use of safer solvents (ethanol instead of methanol), safe and metal-free catalysts, and performing the reaction at room temperature (instead of 60 °C) are the benefits of our study.

4. Conclusion

In the last decade, the use of aerogels has garnered attention due to their porous structure and low synthesis cost. In this research, a carbon nanotube aerogel was synthesized at a low cost and used in a reduction reaction. The aerogels have been prepared by crosslinking the prepared GO with chitosan and freeze-drying. The prepared aerogel material showed appropriate thermal stability, an interesting honeycomb-like structure, high porosity, surface functional group versatility, and high surface area, which all of them are the desired properties for catalytic purposes. Through various analyses and experiments, it was proven that the carbon nanotube aerogel, due to its

mesoporous structure, is a suitable option for catalyzing the reaction of beta-nitrostyrene with hydrazine hydrate via a retro-aza-Henry type reaction. The results of this research demonstrated that this reaction can be carried out with high efficiency at room temperature without the need for heating in 3 h. 11 β -nitrostyrene derivatives were successfully converted to the related hydrazones using the employed catalyst at the optimized conditions. The catalyst showed promising results in the reusability experiments, which after six consecutive runs, the reaction remained almost quantitative.

Authors contributions

Authors have contributed equally in preparing and writing the manuscript.

Availability of data and materials

The data that support the findings of this study are available from the corresponding author, upon reasonable request.

Conflict of interests

The author declare that they have no known competing financial interests or personal relationships that could have appeared to influence the work reported in this paper.

Table 3. The comparison between the present work and related studies.

Catalyst	Solvent	Temp. (°C)	Time (h)	Yield (%)	Ref.
No catalyst	MeOH	60	1	97	[49]
GA (10 mg)	EtOH	r.t.	4	100	[50]
Aerogel (30 mg)	EtOH	r.t.	3	100	This work

References

- [1] A. Du, B. Zhou, Z. Zhang, and J. Shen. *Mater.*, **6** (2013):941–968, . DOI: <https://doi.org/10.3390/ma6030941>.
- [2] S. Chrasekaran, P. G. Campbell, T. F. Baumann, and M. A. Worsley. *J. Mater. Res.*, **32** (2017):4166–4185. DOI: <https://doi.org/10.1557/jmr.2017.411>.
- [3] S. Lyu, H. Chang, L. Zhang, S. Wang, S. Li, Y. Lu, and S. Li. *Comp. Part B: Eng.*, **264** (2023):110888. DOI: <https://doi.org/10.1016/j.compositesb.2023.110888>.
- [4] A. G. Niculescu, D. I. Tudorache, M. Bocioagă, D. E. Mihaiescu, T. Hadibarata, and A. M. Grumezescu. *NanoMater.*, **14** (2024):469. DOI: <https://doi.org/10.3390/nano14050469>.
- [5] H. Gu, X. Huo, J. Chen, S. M. El-Bahy, and Z. M. El-Bahy. *Food Agrorestry*, **10** (2022):1–9, . DOI: <https://doi.org/10.30919/esfaf782>.
- [6] P. Meti, Q. Wang, D. B. Mahadik, K. Y. Lee, Y. D. Gong, and H. H. Park. *NanoMater.*, **13** (2023):1498. DOI: <https://doi.org/10.3390/nano13091498>.
- [7] W. Yao, A. Hu, J. Ding, N. Wang, Z. Qin, X. Yang, and Y. Li. *Adv. Mater.*, **35** (2023):2301894. DOI: <https://doi.org/10.1002/adma.202301894>.
- [8] A. C. Pierre and G. M. Pajonk. *Chem. Rev.*, **102** (2002):4243–4266.
- [9] P. Gu, L. Lu, X. Yang, Z. Hu, X. Zhang, Z. Sun, and G. Zu. *Adv. Func. Mater.*, **34** (2024):2400589, . DOI: <https://doi.org/10.1002/adfm.202400589>.
- [10] A. Yousefi and A. Nezamzadeh-Ejhih. *Iranian J. Catal.*, **11** (2021). URL <https://oicpress.com/ijc/article/view/3600>.
- [11] L. Keshavarz, M. R. Ghaani, J. D. MacElroy, and N. J. English. *Chem. Eng. J.*, **412** (2021):128604. DOI: <https://doi.org/10.1016/j.cej.2021.128604>.
- [12] G. Ror, L. Vlcek, M. S. Gruszkiewicz, A. A. Chialvo, L. M. Anovitz, J. L. Banuelos, and D. R. Cole. *J. Phys. Chem. C*, **118** (2014):15525–15533. DOI: <https://doi.org/10.1021/jp503739x>.
- [13] W. Yang. *Cellulose*, **26** (2019):6449–6476. DOI: <https://doi.org/10.1007/s10570-019-02559-x>.
- [14] Y. Liu, M. Hao, Z. Chen, S. Ramakrishna, Y. Liu, X. Wang, and Y. Wei. *Fuel*, **354** (2023):129338. DOI: <https://doi.org/10.1016/j.fuel.2023.129338>.
- [15] J. Paul and S. S. Ahankari. *Carbohydr. Pol.*, **309** (2023):120677. DOI: <https://doi.org/10.1016/j.carbpol.2023.120677>.
- [16] R. Ganesamoorthy, V. K. Vadivel, R. Kumar, O. S. Kushwaha, and H. J. Mamane. *Clean. Product*, **329** (2021):129713. DOI: <https://doi.org/10.1016/j.jclepro.2021.129713>.
- [17] Y. Wang, Z. Chen, L. Yang, C. Bian, Z. Du, T. Xu, and L. He. *En. Build.*, **320** (2024):114617, . DOI: <https://doi.org/10.1016/j.enbuild.2024.114617>.
- [18] N. Zekri and R. Fareghi-Alamdari. *Iran. J. Catal.*, **14** (2024). DOI: <https://doi.org/10.57647/j.ijc.2024.1401.02>.
- [19] H. Vahabi, F. Gholami, M. Tomas, E. Movahedifar, M. K. Yazdi, and M. R. Saeb. *J. Vinyl Additive Techn.*, **30** (2024):5–25. DOI: <https://doi.org/10.1002/vnl.22041>.
- [20] Q. Zhang, Q. Xu, D. Yang, X. Wang, M. Zheng, Z. Liu, and J. Wang. *Chem. Eng. J.*, (2024):157355. DOI: <https://doi.org/10.1016/j.cej.2024.157355>.
- [21] J. Choi and D. J. Suh. *Catal. Surveys Asia*, **11** (2007):123–133. DOI: <https://doi.org/10.1007/s10563-007-9024-2>.
- [22] C. Kim, K. M. Cho, K. Park, J. Y. Kim, G. T. Yun, F. M. Toma, and H. T. Jung. *Adv. Func. Mater.*, **31** (2021):2102142, . DOI: <https://doi.org/10.1002/adfm.202102142>.
- [23] L. Peles-Strahl, Y. L. Persky, and L. Elbaz. *SusMat*, **3** (2023):44–57. DOI: <https://doi.org/10.1002/sus2.104>.
- [24] K. Gu, E. J. Kim, S. K. Sharma, P. R. Sharma, S. Bliznakov, B. S. Hsiao, and M. H. Rafailovich. *Mater. Today En.*, **19** (2021):100560, . DOI: <https://doi.org/10.1016/j.mtener.2020.100560>.
- [25] J. H. Lee and S. J. Park. *Carbon*, **163** (2020):1–18. DOI: <https://doi.org/10.1016/j.carbon.2020.02.073>.
- [26] H. Yu, S. Oh, Y. Han, S. Lee, H. S. Jeong, and H. J. Hong. *Chemosphere*, **285** (2021):131448. DOI: <https://doi.org/10.1016/j.chemosphere.2021.131448>.
- [27] J. Wang, X. Yang, D. Wu, R. Fu, M. S. Dresselhaus, and G. J. Dresselhaus. *J. Power Sources*, **185** (2008):589–594, . DOI: <https://doi.org/10.1016/j.jpowsour.2008.06.070>.
- [28] P. Hao, Z. Zhao, J. Tian, H. Li, Y. Sang, G. Yu, and A. Umar. *Nanoscale*, **6** (2014):12120–12129. DOI: <https://doi.org/10.1039/C4NR03574G>.
- [29] O. Lori, N. Zion, H. C. Honig, and L. Elbaz. *ACS Catal.*, **11** (2021):13707–13713. DOI: <https://doi.org/10.1021/acscatal.1c03332>.
- [30] X. Ding, M. Li, J. Jin, X. Huang, X. Wu, and L. Feng. *Chin. Chem. Letters*, **33** (2022):2687–2691. DOI: <https://doi.org/10.1016/j.ccl.2021.09.076>.
- [31] S. Xi, Y. Wang, X. K. Zhang, J. Cao, J. Su, J. Shen, and X. Wang. *Pol. Testing*, **129** (2023):108259. DOI: <https://doi.org/10.1016/j.polymertesting.2023.108259>.
- [32] H. J. Kim, W. I. Kim, T. J. Park, H. S. Park, and D. J. Suh. *Carbon*, **46** (2008):1393–1400, . DOI: <https://doi.org/10.1016/j.carbon.2008.05.022>.
- [33] A. Smirnova, T. Wender, D. Goberman, Y. L. Hu, M. Aindow, W. Rhine, and N. M. Sammes. *International J. Hydr. En.*, **34** (2009):8992–8997. DOI: <https://doi.org/10.1016/j.ijhydene.2009.08.055>.
- [34] H. Du, B. Li, F. Kang, R. Fu, and Y. Zeng. *Carbon*, **45** (2007):429–435, . DOI: <https://doi.org/10.1016/j.carbon.2006.08.023>.
- [35] M. Seredych, K. László, and T. J. Bosz. *ChemCatChem*, **7** (2015):2924–2931. DOI: <https://doi.org/10.1002/cctc.201500192>.
- [36] R. Li, T. Gao, P. Wang, W. Qiu, K. Liu, Y. Liu, and P. Li. *Appl. Catal. B: Environ.*, **331** (2023):122677, . DOI: <https://doi.org/10.1016/j.apcatb.2023.122677>.
- [37] X. Tian, M. Zhou, C. Tan, M. Li, L. Liang, K. Li, and P. Su. *Chem. Eng. J.*, **348** (2018):775–785. DOI: <https://doi.org/10.1016/j.cej.2018.05.007>.
- [38] R. Du, N. Zhang, J. Zhu, Y. Wang, C. Xu, Y. Hu, and J. Zhang. *Small*, **11** (2015):3903–3908, . DOI: <https://doi.org/10.1002/sml.201500587>.
- [39] C. C. Wang and S. Y. Lu. *Nanoscale*, **7** (2015):1209–1215. DOI: <https://doi.org/10.1039/C4NR06118G>.
- [40] M. Darrudi, H. Tavakol, and M. M. Momeni. *Int. J. Hydr. En.*, **48** (2023):3495–3510. DOI: <https://doi.org/10.1016/j.ijhydene.2022.10.145>.
- [41] M. T. Jafari-Chermahini, H. Tavakol, and W. Salvenmoser. *ChemistrySelect*, **5** (2020):968–978. DOI: <https://doi.org/10.1002/slct.201904310>.

- [42] F. Hassani and H. Tavakol. *Full. Nanotub. Carbon Nanostruct.*, **26** (2018):479–486.
DOI: <https://doi.org/10.1080/1536383X.2018.1448793>.
- [43] B. Abtahi and H. Tavakol. *ChemistrySelect*, **5** (2020):12582–12585.
DOI: <https://doi.org/10.1002/slct.202003442>.
- [44] M. A. Ranjbari, H. Tavakol, and M. Manoukian. *Res. Chem. Intermed.*, **47** (2021):709–721.
DOI: <https://doi.org/10.1007/s11164-020-04294-6>.
- [45] S. Shamsaddinimotlagh, M. A. Ranjbari, H. Tavakol, and M. Shi. *Synlett*, **35** (2024):1822–1827.
DOI: <https://doi.org/10.1055/a-2239-6819>.
- [46] S. Mallakpour, E. Azadi, and C. M. Hussain. *New J. Chem.*, **45** (2021):3756–3777.
DOI: <https://doi.org/10.1039/D0NJ06035F>.
- [47] A. H. Bashal, K. D. Khalil, A. M. Abu-Dief, and M. A. El-Atawy. *Int. J. Biol. Macromol.*, **253** (2023):126856.
DOI: <https://doi.org/10.1016/j.ijbiomac.2023.126856>.
- [48] K. Li, Q. Liu, H. Cheng, M. Hu, and S. Zhang. *Spectrochim. Acta A*, **249** (2021):119286. .
DOI: <https://doi.org/10.1016/j.saa.2020.119286>.
- [49] A. V. N. Shastin, V. Korotchenko, V. G. Nenajdenko, and E. S. Balenkova. *Tetrahedron*, **56** (2021):6557–6563.
DOI: [https://doi.org/10.1016/S0040-4020\(00\)00606-2](https://doi.org/10.1016/S0040-4020(00)00606-2).
- [50] H. Tavakol and N. J. Abdollahi. *Iran. Chem. Soc.*, **22** (2025):877–887.
DOI: <https://doi.org/10.1007/s13738-025-03194-z>.